GRAVITATIONALLY UNSTABLE FLAMES: RAYLEIGH–TAYLOR STRETCHING VERSUS TURBULENT WRINKLING

E. P. HICKS[1,3] AND R. ROSNER[2]
[1] Center for Interdisciplinary Exploration and Research in Astrophysics (CIERA) and the Department of Physics and Astronomy,
Northwestern University, Evanston, IL 60208, USA; eph2001@columbia.edu
[2] Computation Institute, The University of Chicago, 5735 S. Ellis Ave., Chicago, IL 60637, USA

ABSTRACT

In this paper, we provide support for the Rayleigh–Taylor-(RT)-based subgrid model used in full-star simulations of deflagrations in Type Ia supernovae explosions. We use the results of a parameter study of two-dimensional direct numerical simulations of an RT unstable model flame to distinguish between the two main types of subgrid models (RT or turbulence dominated) in the flamelet regime. First, we give scalings for the turbulent flame speed, the Reynolds number, the viscous scale, and the size of the burning region as the non-dimensional gravity (G) is varied. The flame speed is well predicted by an RT-based flame speed model. Next, the above scalings are used to calculate the Karlovitz number (Ka) and to discuss appropriate combustion regimes. No transition to thin reaction zones is seen at Ka = 1, although such a transition is expected by turbulence-dominated subgrid models. Finally, we confirm a basic physical premise of the RT subgrid model, namely, that the flame is fractal, and thus self-similar. By modeling the turbulent flame speed, we demonstrate that it is affected more by large-scale RT stretching than by small-scale turbulent wrinkling. In this way, the RT instability controls the flame directly from the large scales. Overall, these results support the RT subgrid model.

Key words: hydrodynamics – instabilities – supernovae: general – turbulence – white dwarfs

Online-only material: color figures

1. INTRODUCTION

It is widely believed that an understanding of the explosions of Type Ia supernovae requires a better understanding of Rayleigh–Taylor (RT) unstable (Sharp 1984) deflagrations. Unfortunately, such an understanding is currently only partial. Models for Type Ia supernovae based on the detonation of a white dwarf progenitor require a transition between an initial nuclear deflagration and an eventual detonation of the entire progenitor star; a transition from a deflagration to a detonation is necessary because models that rely on either a deflagration or a detonation alone do not reproduce observations (Arnett 1969; Khokhlov et al. 1993; Khokhlov 1995; Filippenko 1997; Gamezo et al. 1999, 2003, 2004). In such models, initial nuclear deflagrations (e.g., subsonic flames) are RT unstable because the dense fuel sits above lighter burnt ashes in the star's gravitational field. The resulting RT instability affects the flame in two different ways: first, it stretches the flame surface; second, the nonlinear evolution of this stretching process generates turbulence behind the flame front, which back-reacts on the flame surface, wrinkling it further (Vladimirova & Rosner 2005; Zhang et al. 2007). Both stretching and wrinkling add to the surface area of the flame, speeding it up. In the deflagration-to-detonation (DDT) model of Type Ia supernovae, the subsonic flame consequently transitions to a supersonic flame, e.g., a detonation, causing the star to explode (Oran & Gamezo 2007). The details of the DDT, in particular, when and how the transition to detonation occurs, determine critical observables such as nickel production (Gamezo et al. 2003, 2004, 2005; Röpke & Niemeyer 2007; Krueger et al. 2012; Seitenzahl et al. 2013). This transition is still not understood, but one possibility,

the Zel'dovich gradient mechanism (Zel'dovich et al. 1970), depends critically on the details of the conditions produced by the deflagration (Khokhlov et al. 1997, 1999; Oran & Gamezo 2007; Röpke 2007; Röpke & Niemeyer 2007). Without a full understanding of RT unstable flames, the mechanism and final nickel yields of this class of Type Ia supernovae models will remain uncertain.

Ideally, this transition would be studied using full-star simulations. However, the separation of scales in the problem make this unfeasible: the size of the star (approximately Earth-sized) is much too large compared to the width of the flame (10^{-4} to 10^2 cm) to resolve both in the same simulation (Oran 2005). Instead, full-star simulations must include a variety of subgrid models, including, in particular, a subgrid model that gives the speed of the flame below certain scales. There are two different types of such subgrid models, each relying on a particular interpretation of deflagration behavior in the flamelet regime. In one, the turbulent flame speed is set by the RT instability. In the other, the interactions of turbulence with the flame front dictate the flame speed. The question at the heart of this paper is which of these two deflagration subgrid models is more physically appropriate.

In RT-type subgrid models (Khokhlov 1995; Khokhlov et al. 1996; Gamezo et al. 2003, 2004, 2005; Zhang et al. 2007; Townsley et al. 2007; Jordan et al. 2008), the turbulent speed of the flame on an unresolved scale Δ is given by the velocity scale $v_{\mathrm{RT}}(\Delta) \propto \sqrt{g\,A\,\Delta}$ which is naturally associated with the RT instability on scale length $\ell = \Delta$. Here, g is the gravity and the Atwood number is $A = (\rho_{\mathrm{fuel}} - \rho_{\mathrm{ash}})/(\rho_{\mathrm{fuel}} + \rho_{\mathrm{ash}})$, where ρ_{fuel} and ρ_{ash} are the densities of the fuel and the ash. This model for flame behavior is based on the hypothesis that the flame surface is self-similar and self-regulating (Khokhlov 1995; Gamezo et al. 2003; Zhang et al. 2007). Self-similarity means that small parts of the flame behave in a similar way to

---

[3] The Department of Astronomy and Astrophysics, The University of Chicago, Chicago, IL 60637, USA.

the entire flame (and so follow $v_{RT}(\ell) \propto \sqrt{g\,A\,\ell}$ at any given scale, ℓ). Self-regulation means that the overall flame speed will adjust back to the RT scaling if small scales are forced to move at a higher flame speed. The higher speed will burn out small wrinkles in the flame surface, decreasing the flame surface area and returning the flame speed to its RT value. The RT subgrid model states that the large-scale RT instability is the major determinant of the flame speed, and that any small-scale effects of turbulence will be self-regulated away.

The second type of subgrid model is based on the interaction of the turbulence produced by the RT instability with the flame front (Niemeyer & Hillebrandt 1995; Niemeyer & Woosley 1997; Niemeyer & Kerstein 1997; Reinecke et al. 1999; Röpke & Hillebrandt 2005; Schmidt et al. 2006a, 2006b). In this model, the RT instability deforms the flame front, the deformation produces turbulence and the turbulence back-reacts on the flame front to control the final turbulent flame speed. These types of subgrid models are based on the field of turbulent combustion, which generally studies the propagation of a flame through a turbulent velocity field. In that case, to first order, the turbulent flame speed is determined by the root-mean-square (rms) velocity of the turbulent velocity field. More elaborate models have been developed and one rigorous Large Eddy Simulation (LES)-based variant has been adapted for supernova subgrid models by Schmidt et al. (2006a, 2006b). Their model also includes the effects of small-scale buoyancy to incorporate RT effects. These models assume that a flame interacts with turbulence behind it in a similar way as with turbulence in front of it. Whether or not this assumption is true is unknown.

Which subgrid model is superior can only be determined by direct studies of RT unstable flames in isolation, and there have been a variety of such studies. They can be organized by different criteria, beginning with dimensionality. Two-dimensional simulations (Bell et al. 2004; Vladimirova & Rosner 2003, 2005; Zhang et al. 2007) can generally cover more of parameter space, but they are fundamentally limited because the behavior of two-dimensional (2D) turbulence is different from three-dimensional (3D) turbulence. 3D simulations (Zingale et al. 2005b; Zhang et al. 2007; Ciaraldi-Schoolmann et al. 2009; Chertkov et al. 2009) treat the turbulence correctly, but they are computationally expensive and so can only be run for short times and for fewer parameter values. RT flame simulations can also differ in what scale they resolve; some use a subgrid model themselves (Ciaraldi-Schoolmann et al. 2009), others resolve the Gibson scale and the flame width (Bell et al. 2004; Zingale et al. 2005b), and still others resolve down to the viscous scale (Vladimirova & Rosner 2003, 2005; Chertkov et al. 2009). Some simulations use a model flame in a Boussinesq setting (Vladimirova & Rosner 2003, 2005; Chertkov et al. 2009), a thickened model flame in a degenerate setting (Zhang et al. 2007), or a carbon–oxygen flame (Bell et al. 2004; Zingale et al. 2005b; Ciaraldi-Schoolmann et al. 2009). Carbon–oxygen flames are most realistic and directly applicable to supernovae, but model flames can better isolate specific effects, such as RT stretching. Studies tend to focus on either the early, transient phases of flame development (Bell et al. 2004; Zingale et al. 2005b; Zhang et al. 2007; Chertkov et al. 2009) or the later, possibly saturated, stages (Vladimirova & Rosner 2003, 2005; Zhang et al. 2007) when the flame speed varies around a statistically stationary average. The flame in the supernova is more likely to be statistically unsteady, because the star is expanding as the flame propagates, but the question of whether 3D, unconfined flames can saturate is still unresolved.

Thus, which choice is more physically relevant—statistically unsteady or saturated simulations—remains unclear. Even if the flame is only transient in the star, saturated simulations indicate the statistically steady state the flame is approaching, even if it never reaches it. Simulations vary in what parameter values they use and also the combustion regime they probe: flamelets (Bell et al. 2004; Zingale et al. 2005b; Vladimirova & Rosner 2003, 2005; Zhang et al. 2007), thin reaction zones (Bell et al. 2004; Zingale et al. 2005b; Chertkov et al. 2009), or broken reaction zones (Chertkov et al. 2009).

There have also been numerous studies that address other aspects of burning in white dwarfs. These generally fall into two categories: flames moving through pre-existing turbulence and buoyant burning bubbles. Studies of flames moving through fields of turbulence could apply if the initial turbulent convection in the star is very strong. In that case, the flame could be deformed and sped up as it is forced to interact with the turbulent eddies. This is a well-studied problem in classical turbulent combustion theory and a comprehensive list of papers would be too long to include here. A few recent papers that explore turbulent combustion with special reference or applicability to the Type Ia problem include Aspden et al. (2008, 2010, 2011c), Poludnenko & Oran (2010), Poludnenko et al. (2011), and Hamlington et al. (2011, 2012). However, a recent study of the initial convection within the white dwarf shows that the convective turbulence probably is not strong enough to influence the flame directly (Nonaka et al. 2012). Another variation of the turbulent combustion problem is to consider the effect of turbulence created by a carbon flame on a trailing oxygen flame (Woosley et al. 2011; Aspden et al. 2011b). Finally, there has also been interest in studying the initial buoyant burning bubble as a whole (Vladimirova 2007; Zingale & Dursi 2007; Aspden et al. 2011a).

Our simulations add to the body of work on RT unstable flames in isolation and attempt to fill in a mid-range gap in parameter space for model flames. The parameter space here is defined by a non-dimensional gravity, G, and a non-dimensional box size, L (see Section 2). The product GL compares the relative importance of the gravitational force and laminar burning, with high GL being dominated by gravity and low GL being dominated by laminar burning. Vladimirova & Rosner (2003, 2005) explored the laminar flame and wrinkled flamelet regimes in depth and began to penetrate into the corrugated flamelet regime by choosing low values of GL. Chertkov et al. (2009) focused on the transition between broken reaction zones and thin reaction zones by choosing very high values of GL. We probe the more turbulent regions of corrugated flamelet regime and look for the transition to the thin reaction zone regime by filling in the parameter space gap and focusing on intermediate values of GL. The corrugated flamelet regime is key for supernova studies, because the flame is expected to spend a significant fraction of its time in this regime. The transition between corrugated flamelets and thin reaction zones is important because it could lead to conditions that may cause a detonation.

This paper gives the results of a parameter study of a simple, 2D, model flame. Because our focus is on reaching an understanding of what effects dominate the flame speed, we neglected many of the complications of white dwarf flames. Thus, instead of a full chemical reaction chain, we used a simple model reaction. Also, we used the Boussinesq approximation, and therefore ignored compressibility effects and sound waves. These simplifications allowed us to focus directly on the effect

that gravity has on the flame without having to disentangle it from other effects. This allows us to compare our results with the those from carbon–oxygen flame studies, such as Bell et al. (2004) and Zingale et al. (2005b), and point out differences. We also focused specifically on the saturated state. In the saturated state, burning and the RT instability balance each other and so the quantities that we are measuring vary around a statistically stationary average. By focusing on the saturated state, we can obtain robust scalings with G that do not depend on time. In these simulations, the flame is forced into a saturated state by the presence of the boundaries. Because the study is in 2D, an inverse energy cascade forces the integral scale of the turbulence to the largest possible size—the size of the domain. In essence, the domain "freezes" the evolution of the flame at a certain scale, allowing it to be studied. The simulations resolve both the flame width and the viscous scale so that the effects of turbulence on the flame are fully accounted for. We focus on the transition from an ordered flame to a highly disturbed one. In effect, we extend the results of Vladimirova & Rosner (2003, 2005) for model flames from the ordered regime into the parameter range where the area behind the flame is turbulent and wrinkles the flame front.

We used this parameter study to look for evidence to support either of the two types of subgrid model. We do not test the subgrid models directly because their formulations can be very complex. After giving the problem formulation in Section 2, we calculate the turbulent flame speed in Section 3, look for a transition between the flamelet and thin reaction zones regimes in Section 4, and test the self-similarity of the flame by calculating its fractal dimension in Section 5. Continuing in Section 5, we assemble a model for the turbulent flame speed based on the fractal nature of the flame and use this model to assess the relative strength of large-scale stretching and small- to mid-scale turbulent wrinkling.

2. THE PROBLEM FORMULATION

Instead of solving the fully compressible Navier–Stokes equation, and continuity and heat equations, we reduced them with the Boussinesq approximation. The Boussinesq approximation only holds when the flow is subsonic, when the scale height of the system is large compared to the vertical scale of the flow and when temperature variations are small (Spiegel & Veronis 1960). In this case, density variations are only taken into account in the gravity term of the Navier–Stokes equation and the continuity equation takes the incompressible form. Although the continuity equation is incompressible, the volume expansion term in the heat equation is taken into account because it is not negligible compared with other heat equation terms. This approach neglects the correction to the inertia term of the momentum equation due to density variations, the viscous dissipation of energy and shocks.

We simulated the Boussinesq fluid equations with a reaction term, $R(T)$, added to the heat equation to model the burning process. $R(T)$ describes the evolution of the fluid from an unburnt fuel at temperature $T = 0$ to burnt ashes at temperature $T = 1$. We chose a model reaction $R(T) = 2\alpha T^2(1 - T)$. This specific model reaction is a form of the bistable reaction with $T_{\text{ignition}} = 0$, so no actual bistable behavior occurs.

This reaction has a very simple laminar solution in a stationary, gravity-free fluid (Constantin et al. 2003). When the flame is laminar, it is completely flat with a characteristic width of δ and it moves with the laminar flame speed s_o. δ and s_o are set by α, the laminar reaction rate, and κ, the thermal diffusivity,

so that $s_o = \sqrt{\alpha\kappa}$ and $\delta = \sqrt{\kappa/\alpha}$. The actual flame thickness (δ_t) is larger than the characteristic flame width (δ) by a factor of 4, $\delta_t = 4\delta$. We calculated δ_t by measuring the distance between the level sets $T = 0.1$ and $T = 0.9$. The bistable reaction was selected because it has a smaller flame thickness than the more commonly used Kolmogorov–Petrovsky–Piskounov (KPP) reaction, which has $\delta_t = 18\delta$ (Vladimirova et al. 2003). We required a thin flame to investigate the effect of wrinkling on the flame front (see Section 5). To measure the flame speed, we calculated the bulk burning rate, which measures the total creation of burned material per unit time (Vladimirova et al. 2003).

The fluid equations were non-dimensionalized by the characteristic length scale (laminar flame front thickness, δ) and timescale in the problem (the reaction time, $1/\alpha$) (Vladimirova & Rosner 2003) to give

$$\frac{D\mathbf{u}}{Dt} = -\left(\frac{1}{\rho_o}\right)\nabla p + GT + \text{Pr}\nabla^2\mathbf{u} \tag{1a}$$

$$\nabla \cdot \mathbf{u} = 0 \tag{1b}$$

$$\frac{DT}{Dt} = \nabla^2 T + 2T^2(1 - T). \tag{1c}$$

Non-dimensionalizing the equations yields two control parameters:

$$G = g\left(\frac{\Delta\rho}{\rho}\right)\frac{\delta}{s_o^2} \tag{2}$$

$$\text{Pr} = \frac{\nu}{\kappa}, \tag{3}$$

where G is the non-dimensionalized gravity and Pr is the Prandtl number. To simplify the problem, physical characteristic values, such as ν (the kinematic viscosity) and κ, are taken to be constants independent of temperature. G is positive if the flame is moving upward out of a gravitational well, as is the case here and in the white dwarf.

There are also several implicit control parameters. These control parameters do not result from non-dimensionalizing the equations, but from our setup. The non-dimensional box size, $L = \ell/\delta$, must be considered because we simulate in a finite computational domain. The Lewis number, Le $= \kappa/D$ (where D is the material diffusivity), is effectively Le $= 1$ because the simulations only track temperature and do not separately consider any material diffusivity. The densimetric Froude number, $\text{Fr}_d = 1/\sqrt{GL}$, gives the relative importance of the gravitational force. Our simulation scenario implicitly assumes that, for large values of GL, only the product GL is physically important. We directly calculate the Reynolds number, Re $= U_{\text{rms}}L$, using U_{rms} calculated from the simulation results, as a measure of the turbulence just behind the flame front. In short, this set of simulations is a parameter study in one variable: only G is varied. Pr, L, and Le are held fixed with the values of Pr $= 1$, $L = 128$, and Le $= 1$.

All simulations used Nek5000 (Fischer et al. 2008), a freely available, open-source, highly scalable spectral element code currently developed by P. Fischer (chief architect), J. Lottes, S. Kerkemeier, A. Obabko, and K. Heisey at the Argonne National Laboratory. Nek5000 has several advantages. The code is fast, has a low memory footprint and efficient preconditioners. Because it is based on spectral elements, its numerical accuracy converges exponentially as the spectral order increases.

Table 1
Simulation Parameters

G	Elements	N_{elem}	l_x	$N_{collocation}$	Physical	Total Time	t_{step}	t_{out}	N_{steps}	Resolution
1	16×336	5376	8	344064	128×2688	510	0.006	1.02	85000	1
2	16×192	3072	10	307200	128×1536	265.2	0.003	1.02	88400	0.8
4	32×448	14336	8	917504	128×1792	204	0.0015	0.51	136000	0.5
8	32×576	18532	8	1179648	128×2304	199.155	0.0015	0.1275	132770	0.5
16	32×512	16384	8	1048576	128×2048	127.5	0.00075	0.255	170000	0.5
32	32×608	19456	10	1945600	128×2432	102	0.0003	0.102	340000	0.4
64	64×1344	86016	8	5505024	128×2688	95.625	0.0001875	0.06375	510000	0.25
128	64×1344	86016	8	5505024	128×2688	67.32	0.00012	0.0612	561000	0.25

Notes. Simulation parameters. The columns are: the non-dimensional gravity, the number of elements in the x- and y-directions, the number of collocation points in the x-direction (l_x^2 is the number of collocation points per element), the total number of collocation points, the physical dimensions, the total running time, the time step, the amount of time between output files, the total number of steps, and the simulation resolution (the average spacing between collocation points). All quantities are non-dimensional.

Nek5000 also allows direct control over the parameters in our problem.

The simulation setup was as follows. The boundary conditions were periodic on the side walls for all of the simulations. The flame moved upward in the box in the direction opposite that of gravity. The top of the simulation domain was subject to an inflow condition with $u_x = 0$ and $u_y = -v_{shift}$. Similarly, the bottom of the simulation domain had an outflow condition with $u_x = 0$ and $u_y = -v_{shift}$. We dynamically set v_{shift} equal to the flame speed at the previous time step, which is permitted by extended Galilean invariance (Pope 2000). The temperature was held at $T = 0$ (fuel) for the top boundary and $T = 1$ (ash) for the bottom boundary. The flame was not allowed to approach either boundary. Initially, the flame was perturbed by a randomly seeded group of waves with an amplitude of 3.0 and wavenumbers between 4.0 and 16.0. The initial temperature profile was given by $T = 0.5*(1.0-\tanh(2.0*r/w))$, where r is the vertical position of the flame front given by the perturbation and w is the initial width of the front, set to $w = 4.0$ for the bistable reaction.

The parameters for all of our simulations are given in Table 1. The total running time for each simulation was chosen so that the flame speed would undergo at least five oscillations of its dominant period after the flame had reached a statistically steady state. The flame speed as a function of time in the statistically steady state is shown in Figure 1 for various values of G. We defined the statistically steady state as beginning when a Reynolds number based on the U_{rms} averaged in a box of size 128×128 placed just below the lowest extent of the flame surface (defined by $T = 0.5$) reached 80% of its first maximum value. All averages, such as the average flame speed or the average fractal dimension, were computed beginning at this time.

We checked that our simulations were fully resolved in three different ways. First, we calculated the viscous scale from the Reynolds number and ensured that the resolution was at least three times smaller than this calculated value. Second, we calculated the fractal dimension (see Section 5.1) and showed that the inner cutoffs are slightly higher than the calculated viscous scale. Finally, we ran lower resolution versions of the same simulations, and found no significant changes in the calculated averaged quantities.

3. SCALING RESULTS

In this section, we show how several quantities scale with changes to the non-dimensional gravity, G. These quantities are the average turbulent flame speed, the average Reynolds number,

the average viscous scale, and the average flame height. We apply our first test of the subgrid models and determine that the scaling of average turbulent flame speed, s, is consistent with the RT subgrid model, but not with a simplified turbulence subgrid model given by $s = U_{rms}$. Visualizations of the temperature field for the simulations are given in Figure 2 and of the vorticity field in Figure 3. These figures show that the flame front becomes stretched and wrinkled for higher values of G. It is this stretching and wrinkling that leads to the scalings that will be given in this section.

The average turbulent flame speed is the most important measured quantity for studies of Type Ia supernovae invoking a DDT transition. Khokhlov (1995) suggested that the turbulent flame speed for an RT-driven flame should scale (in our dimensionless units) as

$$s = s_o\sqrt{0.125GL} \qquad (4)$$

for large enough values of G and L. This result is derived directly from the growth rate of the RT instability found by linear perturbation theory. This equation implies that the turbulent flame speed should be independent of the laminar flame speed. Zhang et al. (2007) confirmed this independence for a carbon–oxygen flame. They also checked Khokhlov's suggested flame speed for the equivalent values of $GL = 400, 671, 1493, 2786$, and found agreement to within 10% of the values predicted by Equation (4). Vladimirova and Rosner checked the scaling for values up to $GL = 128$ for reflecting boundary conditions (Vladimirova & Rosner 2003) and $GL = 512$ for periodic boundary conditions (Vladimirova & Rosner 2005). They also found a correction to Khokhlov's prediction at low values of G, and obtained

$$s = s_o\sqrt{1 + 0.0486(G - G_1)L}, \qquad (5)$$

where $G_1 = 8(2\pi/L)^{1.72}$ is roughly the transition point between the planar and cusped flames (Vladimirova & Rosner 2003). This is equivalent to Khokhlov's prediction, except with a slightly different constant due to the measurements being in 2D instead of 3D.

Our set of simulations tests the scaling law for a wider range of GL than either of these previous studies in the flamelet regime, up to $GL = 16,384$. Our best fit for the average flame speed (see Figure 4(a)) is

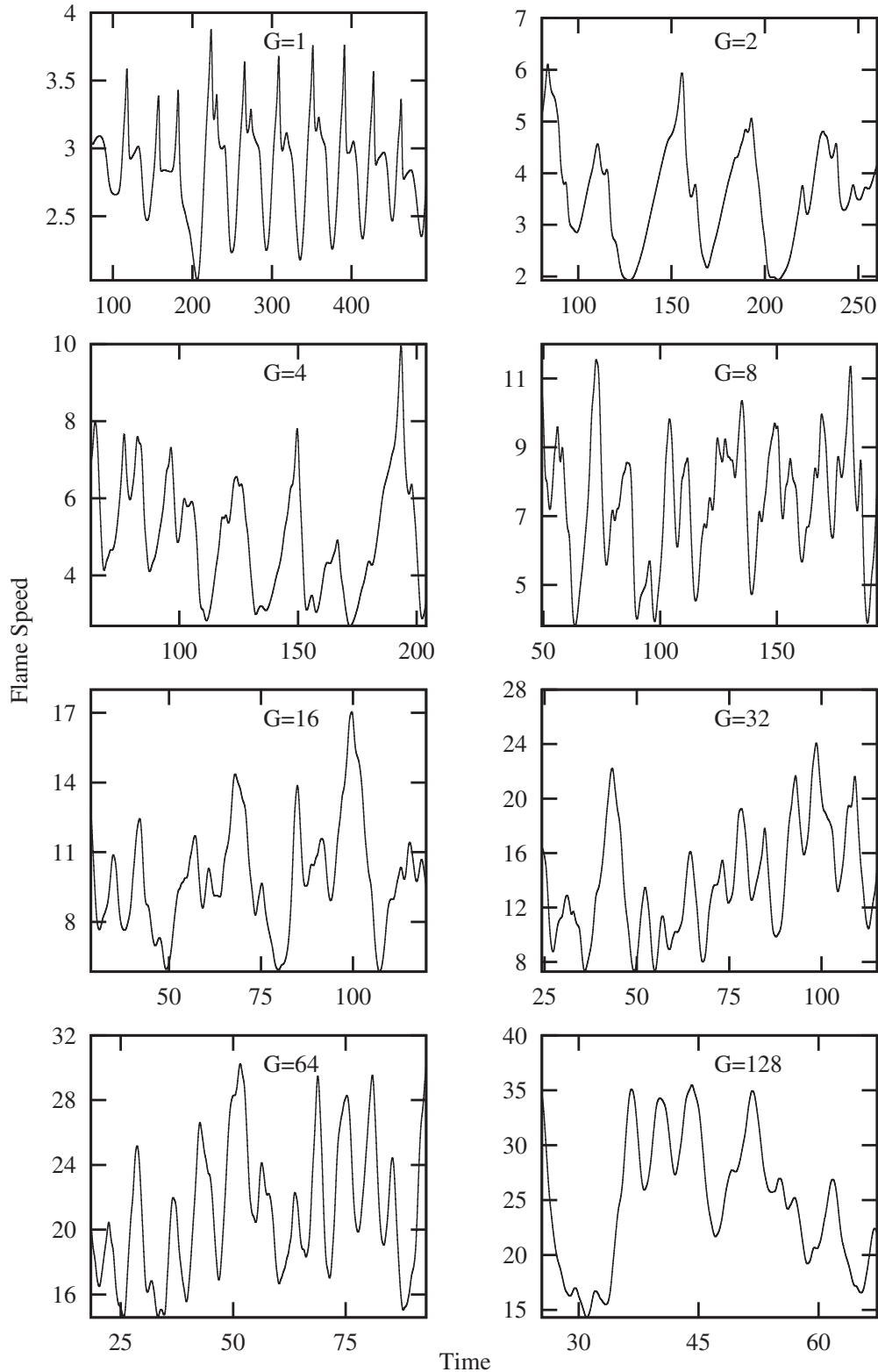$$s = s_o (1 + 0.0656(G - G_1)L)^{0.471}, \qquad (6)$$

Figure 1. Turbulent flame speed in the statistically steady regime as a function of time for various values of G. Initial transients are not shown.

which is very close to the predicted scaling of $\sqrt{GL}$. If we assume that the predicted scaling is true, then we find

$$s = s_o\sqrt{1 + 0.0503(G - G_1)L}. \tag{7}$$

For this and all of our other scalings, we use the basic form given in Equation (5) and assume that the same dependencies on G_1

and L hold. (We have not yet extended this study to different values of L to test these assumptions, but plan this for future work.) The constant ($k_1 = 0.0503$) in Equation (7) is consistent with Vladimirova and Rosner's result, $k_1 = 0.0486$, rather than Khokhlov's, $k_1 = 0.125$, as expected from the dimensionality difference. The constant also matches the prediction for the speed of a Boussinesq 2D rising bubble (Bychkov & Liberman

5
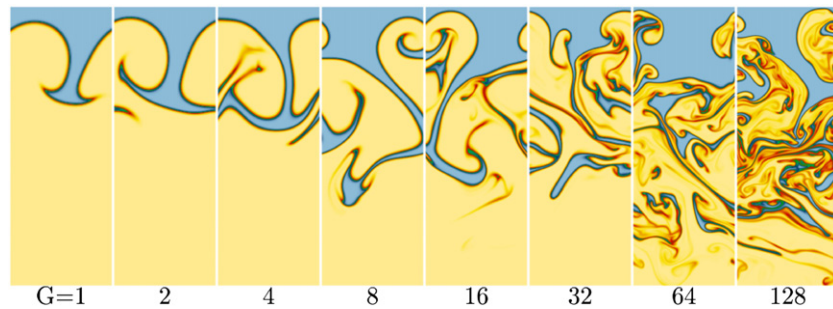
Figure 2. Temperature field for various values of G. Blue is fuel (T = 0) and yellow is ash (T = 1). Intermediate temperature values (which can be seen for the higher values of G) are green and red. The flame moves upward against the direction of gravity, which is downward. The computational boxes are much larger than those shown here.

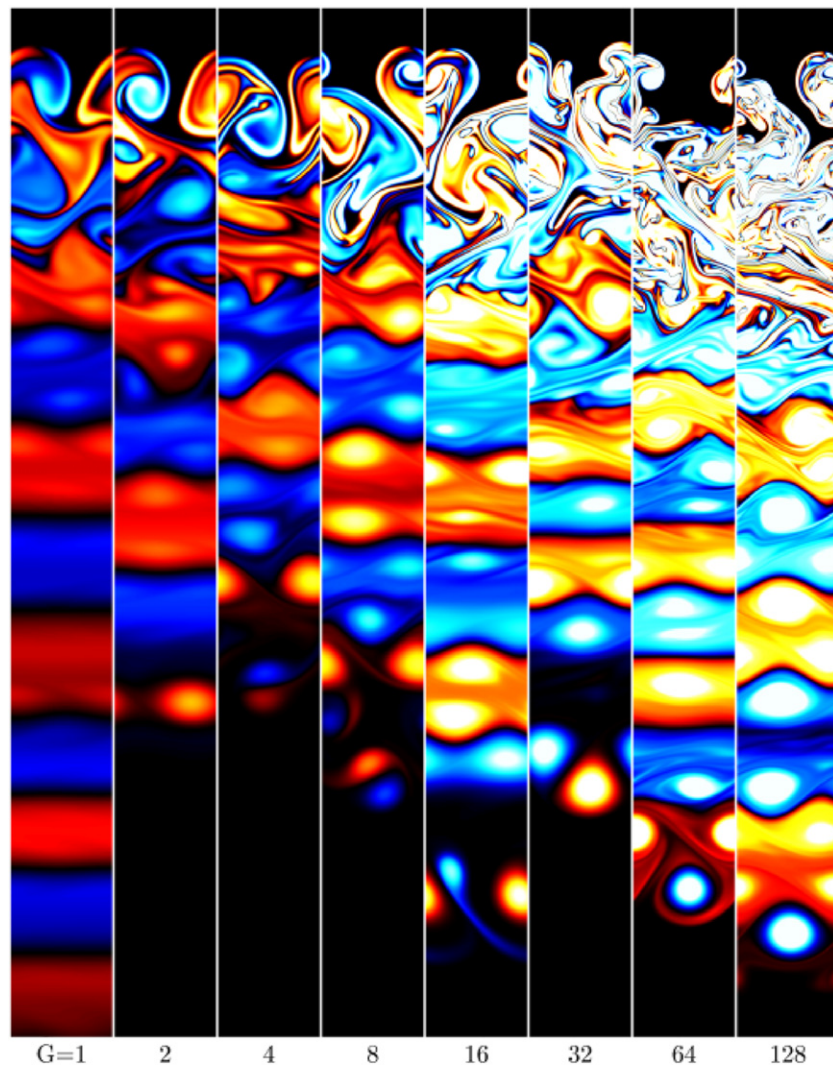(A color version of this figure is available in the online journal.)

Figure 3. Vorticity fields for various values of G. Red vorticity points out of the page and blue vorticity points into the page. Lighter shades indicate stronger vorticity. The layering seen downstream of the flame surface is due to the merger of vortices shed by the flame. These mergers are encouraged by the periodic boundary conditions. The layers are left behind by the flame front and do not affect the flame front evolution. These vorticity layers should not be confused with the pathological layering of density seen in simulations of the Rayleigh–Taylor instability without burning. These simulations are far from that regime, because the effect of burning is still strong here.

(A color version of this figure is available in the online journal.)

2000; Layzer 1955), as pointed out by Vladimirova & Rosner (2003). This similarity between our result and Vladimirova's suggests that the KPP reaction and the bistable reaction have roughly the same flame speed at or above G = 1. Overall, these results confirm that the appropriate subgrid model for

an RT-driven flame in 2D is the RT flame speed, as given by Equation (7).

We also measured the Reynolds number in the area between the uppermost and lowermost extent of the T = 0.5 temperature contour. This is the area where the turbulence is directly next to
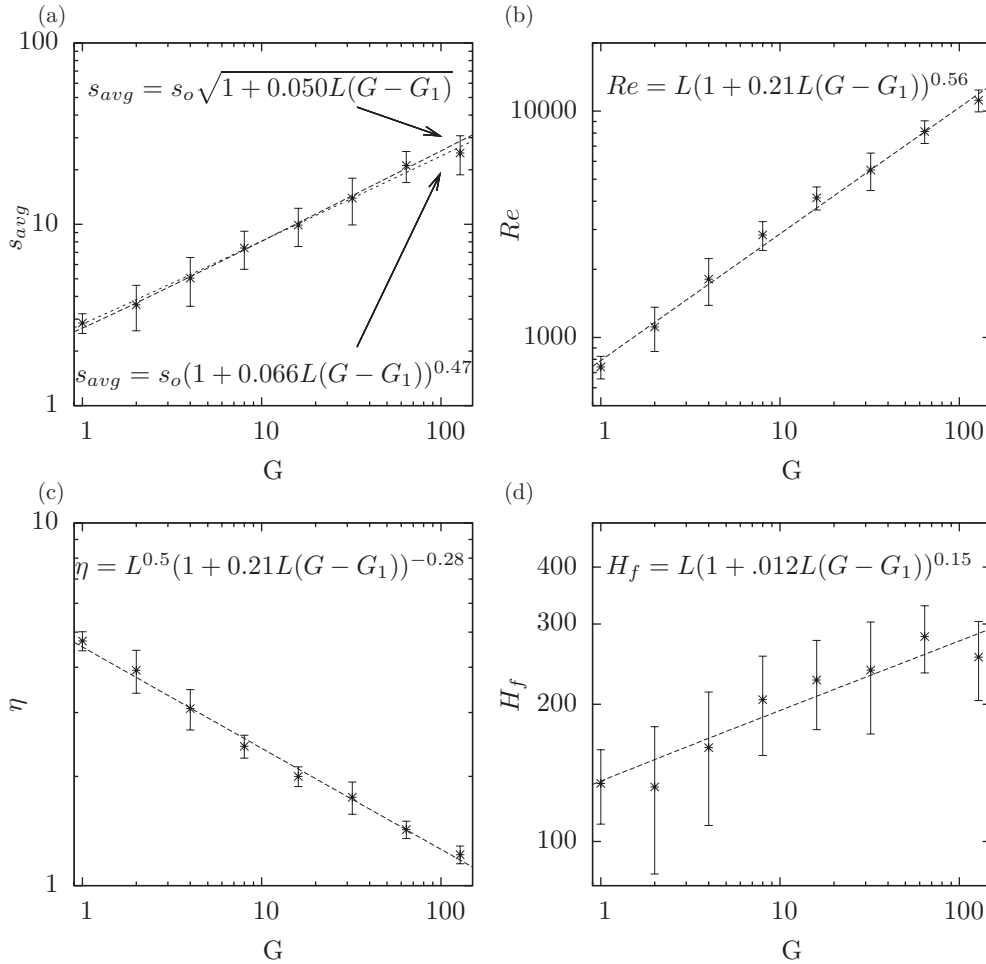
Figure 4. (a) Average flame speed as a function of G. This plot shows the best fit, which scales as $(GL)^{0.471}$, and the fit predicted from theory, $\sqrt{GL}$. (b) The Reynolds number as a function of G, and the best-fit curve. The Reynolds number is calculated using the box size (L) and the rms velocity between the top and bottom of the $T = 0.5$ contour and below the flame front. (c) The viscous scale as a function of G as calculated from $\eta = L\mathrm{Re}^{-1/2}$. The actual laminar flame thickness is $\delta_t = 4$. (d) The flame height as a function of G. The flame height is the vertical distance between the highest and lowest occurrences of the $T = 0.5$ contour. In all four graphs, the error bars show the standard deviation of the oscillations around the average value of the quantity.

the flame front. When the flame is turbulent the largest eddies are of size L, so $\mathrm{Re} = U_{\mathrm{rms}}L/\nu$. The results are shown in Figure 4(b), and the best-fit scaling is

$$\mathrm{Re} = L\left(1 + 0.205(G - G_1)L\right)^{0.558}. \qquad (8)$$

This suggests that subgrid models of the form $s = U_{\mathrm{rms}}$ overestimate the flame speed significantly (by a factor of three for $G = 128$). The fact that $U_{\mathrm{rms}} > s$ also shows that the turbulence behind the flame must interact with the flame front—the flame cannot outrun it entirely. It is also important to note that U_{rms} cannot be predicted on its own. An unphysical flame, for instance, the very artificially thickened flame used in many supernovae simulations, could produce an incorrect U_{rms} and therefore an incorrect prediction for the flame speed.

The viscous scale was calculated directly from the Reynolds number data using the viscous scale in 2D turbulence: $\eta = L\mathrm{Re}^{-1/2}$. The best-fit scaling for the viscous scale (see Figure 4(c)) is

$$\eta = L^{0.5}\left(1 + 0.207(G - G_1)L\right)^{-0.280}. \qquad (9)$$

The viscous scale is smaller than our actual laminar flame thickness ($\delta_t = 4$) for $G > 2$. This will become important

in Section 5.2 which concerns a fractal model for the flame speed.

The flame height is the amount of vertical space which contains burning, here defined as the vertical distance between the top and bottom of the $T = 0.5$ temperature contour. It scales as

$$H_f = L\left(1 + 0.012(G - G_1)L\right)^{0.152}; \qquad (10)$$

see Figure 4(d). This is in contrast to the results of Vladimirova & Rosner (2005) and Zhang et al. (2007), who found that the height of the flame brush was roughly twice the width of the box and independent of G.

In this section, we showed that the flame follows the RT scaling for the flame speed, even in the limit when the flow behind the flame is quite turbulent (Re $\sim$ 10,000). An alternative model, based on the turbulent velocity behind the flame front, overpredicts the flame speed. We confirmed that the bistable reaction moved at similar speeds to the KPP model reaction given in Vladimirova & Rosner (2003, 2005), so we do not expect that the RT scaling is flame model-dependent. We also gave scalings for the average Reynolds number, the average viscous scale, and the average flame height. The average flame height does vary with G, in contrast to previous results. The

flame speed scales as the RT flame speed, which supports the RT subgrid model, at least in the 2D case we have explored.

4. COMBUSTION REGIMES

In this section, we consider whether the simulations show a transition between the "corrugated flamelet" and "thin reaction zones" regimes of traditional turbulent combustion theory (Peters 2000). If this transition does not occur when predicted, it could mean that the traditional turbulent combustion theory upon which these regimes, and turbulence-based subgrid models, are based does not apply to RT unstable flames. The transition is predicted to occur at Ka $= (\tau_c/\tau_t) = 1$, where Ka is the Karlovitz number. In the corrugated flamelet regime, the chemical timescale (τ_c) is shorter than the turbulent timescale (τ_t), and so Ka < 1. The flame is wrinkled by turbulence, but its internal structure remains intact because the viscous scale is larger than the flame width. When Ka > 1, in the thin reaction zones regime, the viscous scale is smaller than the flame width and the internal flame structure changes.

We calculated the Karlovitz number to find the value of G at which the transition from corrugated flamelets to the thin reaction zones regime should occur. The Karlovitz number is based on the distance between the $T = 0.1$ to $T = 0.9$ temperature contours, 4δ for the bistable reaction. So

$$\mathrm{Ka} = \frac{\tau_{aw}}{\tau_t} = \left(\frac{4\delta}{s_o}\right)\left(\frac{U_{rms}}{L}\right) = \frac{4\left(1 + 0.205(G - G_1)L\right)^{0.558}}{L},$$

(11)

where we used the scaling for the Reynolds number given by Equation (8). Here, τ_{aw} is the chemical crossing timescale for the actual width of the flame, measured between the $T = 0.1$ and $T = 0.9$ temperature contours. We also used the fact that, for 2D turbulence, eddies of all sizes have the same characteristic turnover time (Davidson 2004, p. 581–582). For large values of G, this Karlovitz number is approximately Ka $\approx (1.68G^{0.56}/L^{0.44})$.

From Equation (11), the transition from corrugated flamelets to thin reaction zones should occur at $G = 18$. Thus, for $G = 1, 2, 4, 8, 16$ the flames should be in the flamelet regime and for $G = 32, 64, 128$ the flames should be in the thin reaction zones regime. However, all of our flames visually appear to remain in the flamelet regime, with just a bit of extra thickening for higher values of G (see Figure 2). Because the transitions between turbulent combustion regimes are only predicted approximately (Law 2006; Poludnenko & Oran 2010), our result should be regarded as only weak evidence of inconsistency with these predictions. That is, for $G = 128$, Ka $= 3$, which is similar enough to the predicted transition value of Ka $= 1$ (given the approximate nature of the theory) that we cannot definitely claim that a transition ought to have taken place.

What other reasons could there be for seeing no transition? One obvious possibility is the properties of the model flame. Because of the nature of the model reaction, there are no separate pre-heat and reaction zones because the bistable reaction allows fuel of any nonzero temperature to burn. Also, the flame cannot become extinct by quenching in a realistic way (see Vladimirova et al. (2003) for a discussion of this point for the KPP reaction). Physically more appropriate flame models tend to be based on models such as the Arrhenius reaction, for which the reaction vanishes exponentially for low temperatures. The bistable reaction has a much less precipitous drop-off in the reaction rate for low temperatures. This means that the transition to the thin reaction zones should be easier than for the Arrhenius reaction, but the subsequent transition to the "broken reaction zones" regime (when the innermost reaction zone is disturbed by turbulence) is unrealistically difficult for these flames. Our simulations, therefore, do not probe this regime, and thus, as long as the transition to thin reaction zones depends mainly on the disruption of the reaction, and not on the extinction of the flame, it actually should occur more easily for model flames.

The second possibility is that traditional turbulent regimes are not appropriate for RT unstable flames because the flame is not forced to completely interact with any given eddy. In traditional turbulent combustion, the turbulence is in the path of the flame (i.e., is already present in the unburnt fuel) so the eddies must move completely through the flame front. (In such situations, the turbulence is typically driven by some mechanism other than the flame itself, although the flame might modify the turbulent flow.) The eddies in our simulation are instead created either within the flame, in front of, or behind the flame, so if they are quickly forced downstream, flame front wrinkling will be minimized—an effect we observed with our simulated flames. In fact, we found that the vorticity ahead of the flame front is negligible compared with the vorticity within and behind the flame for all of our simulations. Given these differences in physical situation, it appears likely that the results from traditional turbulent combustion cannot be simply applied to an RT-driven flame. That the bistable flames studied here remained in the flamelet regime, and did not transition to the thin reaction zones regime, suggests that the traditional turbulent flame picture does not apply here. It further suggests that if a turbulent flame model is to be developed for such flames, substantial modifications to the traditional theory will be required. In any case, the above arguments cast doubt on the applicability of the turbulence-based subgrid model, since it is based on the very physical mechanisms that underlie the traditional combustion regimes.

5. MEASURING WRINKLING WITH THE FRACTAL DIMENSION

Given that the turbulence-based subgrid model appears to be an unlikely candidate for the kinds of flames we have investigated, we next need to test whether the alternative RT subgrid model is physically consistent with our simulation results. We perform this test in the present section: we test the self-similarity requirement for the RT subgrid model by checking whether the flames are fractal. Gouldin (1987) applied the theory of fractals to turbulent flames for the first time and many other studies have made the same application since, for example, Kerstein (1988), Mantzaras et al. (1989), Gulder (1990), Woosley (1990), Bravo & Garcia-Senz (1995), Collins (1995), Blinnikov & Sasorov (1996), Gulder (1999), and Sreenivasan (2004). As we will show, our simulated flames are indeed fractal; furthermore, we will show that the fractal dimension increases with G up to an asymptotic value of roughly $D_F \approx 1.5$. This sort of asymptotic behavior is naturally expected from passive scalar theory. Using the asymptotic value for the fractal dimension and the flame's fractal behavior, we construct a fractal model for the flame speed. Finally, we show that a larger fraction of the flame speed comes from large-scale stretching than from small-to-mid-scale turbulent wrinkling.

5.1. Calculating the Fractal Dimension of the Flame Front

A fractal is defined as an object "whose parts relate to the whole in some way" (Sreenivasan 1991). Put another way, a

fractal (curve) is an object whose measured length changes depending on what size ruler is used to measure it (Mandelbrot 1967, 1982). For a true fractal curve, the length becomes infinite as a ruler size goes to zero. The total number of rulers, N, needed to cover a curve measured at a scale ϵ is given by

$$N(\epsilon) = \epsilon^{-D_F}. \tag{12}$$

This leads to an expression for the fractal dimension

$$D_F = -\lim_{\epsilon \to 0} \frac{\log(N(\epsilon))}{\log(\epsilon)}. \tag{13}$$

A common way to measure the fractal dimension is to compute the box counting (or capacity) dimension (Sreenivasan & Meneveau 1986). The box counting algorithm uses boxes of different sizes (instead of rulers) to measure the length of the curve. For each box size, the space that the curve is embedded in is tiled with boxes. The minimum number of boxes of each size needed to cover the curve is counted. This minimum is found by repeating box counting several times with the same box size but with the boxes in different positions. After recording the number of boxes for a range of box sizes, a plot is made of the log of the number of boxes at each size versus the log of the box sizes. The slope of this plot is the fractal dimension. We applied a box counting algorithm to the $T = 0.5$ temperature contour to find the fractal dimension of the flame fronts. For each box size, we used the maximum number of possible offsets allowed by the simulation resolution to find the minimum number of boxes for each box size. Each simulation output file was measured separately. To find the fractal dimension for a given value of G, we averaged over the fractal dimension for each file in the same time range that was used to find the average velocity.

For physical objects, including flames, there is an inner cutoff scale below which no extra length will be measured. For example, if wrinkling is caused by turbulence, then there should be no extra wrinkling at scales below the viscous scale. Physical objects also have a maximum scale, the outer cutoff scale, below which the curve exhibits fractal behavior. In the case where both the inner and outer cutoff scales exist, a total, true length can be measured for the curve. This true length is the length of the curve measured with a ruler the size of the inner cutoff scale. In terms of the fractal dimension and the inner and outer cutoff scales, this length is given by (Sreenivasan 1991)

$$L_f = L_o * \left(\frac{L}{\eta}\right)^{D_F - 1}, \tag{14}$$

where η is the inner cutoff scale, L is the outer cutoff scale (in this case, the box width), D_F is the fractal dimension, and L_o is the length measured with a ruler the size of the box width, L.

In order to find the actual length of the flame (and therefore calculate the flame speed), the inner and outer cutoffs must be known. We found that the inner cutoff occurs somewhere between the viscous scale and the flame width. The fractal behavior is clear between the flame width and around 50%–60% of the total simulation size, L. This is about the box size at which the box counting procedure usually begins to fail (Foroutan-pour et al. 1999). The failure of box counting to find fractal similarity above a certain box size does not mean that the object is not fractal on these scales. If the object is very convoluted on the largest scales, as flames are, then box counting will undercount the number of ruler lengths necessary to measure the flame
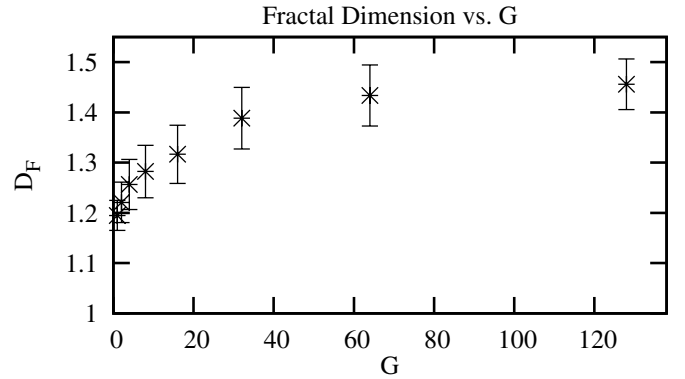

Figure 5. Fractal dimension as a function of G. The error bars indicate the standard deviation of the oscillations of the fractal dimension around the average fractal dimension. The fractal dimension appears to asymptote to approximately $D_F = 1.5$ for high values of G.

length at these scales. In our fractal model in Section 5.2, we will assume that fractal behavior extends all the way from the viscous scale to the integral scale (L).

As shown in Figure 5, we find that the average fractal dimension is larger for larger values of G. (The error bars indicate the standard deviation of the fractal-dimension measurements.) This variation in fractal dimension for a given G is probably natural and not due to measurement uncertainties. Similar variation has been seen in other fractal systems that are generated by turbulence (Prasad & Sreenivasan 1989). Sreenivasan (1991) proposed that it is due to the probabilistic nature of the turbulence itself.

The fractal dimension seems to asymptote toward $D_F \approx 1.5$ for large values of G. It is physically likely that such a firm asymptote below $D_F = 2$ does exist. We expect this from studies of the interfaces of passive scalars in turbulent flows in 3D. Experimental studies (summarized in Sreenivasan 1991) show that the fractal dimension of such scalar interfaces tends to approach $D_F = 2.36$ for high Reynolds numbers. Sreenivasan et al. (1989) calculated an asymptotic fractal dimension very similar to this ($D_F = 7/3$) theoretically by considering the momentum flux across the interface. In addition, Constantin et al. (1991) calculated an absolute upper limit of $D_F = 2.5$ for scalar isosurfaces. Such limits probably also exist for scalar surfaces in 2D. Of course, the temperature field of the flame is not a passive scalar, so these arguments do not directly apply. However, for large values of G the behavior of the temperature field becomes increasingly like that of a passive scalar because the chemical timescale becomes much longer than the hydrodynamic timescale. This means that arguments for upper limits of the fractal dimension for scalar isosurfaces should apply for large values of G, and so the fractal dimension should reach an asymptotic value considerably below $D_F = 2$.

To conclude, in this subsection we showed that the simulated flames are fractal, and that the fractal dimension increases with G up to an asymptotic value of roughly $D_F \approx 1.5$. We also put forth an argument for why we expect that the fractal dimension should be asymptotic toward an intermediate value between $D_F = 1$ and 2 instead of increasing to $D_F = 2$. The fact that the flames are fractal means that they are self-similar—this is consistent with one of the properties of the RT subgrid model, and thus supports its applicability to the kinds of flames we have studied here.

5.2. Large-scale Rayleigh–Taylor Stretching versus Turbulent Wrinkling

The effects of large-scale RT stretching and turbulent wrinkling on the flame front can be disentangled by finding their respective contributions to the flame area and therefore the flame speed. In this subsection, we construct a model for the flame speed based on the fractal behavior of the flame and extract the contributions from wrinkling and stretching. We then examine how this argument might be extended to 3D. Finally, we comment on the effects of local flame stretch and curvature, which could potentially destroy the proportionality between the flame surface area and the flame speed.

Damkohler (1940, 1947 translation) suggested that the flame speed for flames in the flamelet regime is directly proportional to the surface area of the flame and is given by

$$\frac{s}{s_o} = \frac{A_f}{A_o}, \tag{15}$$

where s is the turbulent flame speed, s_o is the laminar flame speed, A_f is the turbulent flame area, and A_o is the undisturbed flame area. This expression assumes that each infinitesimal piece of flame surface moves with the laminar flame speed. Models that use fractals to determine the flame surface area have since been considered by Kerstein (1988), Mantzaras et al. (1989), Gulder (1990, 1999), Woosley (1990), Collins (1995), Blinnikov & Sasorov (1996), and Sreenivasan (2004).

Since our simulations are in 2D, the flame area is really a flame length. Using Damkohler's model for the flame speed, $s/s_o = L_f/L$, a fractal model for the flame area is

$$L_f = L_{\mathrm{RT}}(G) * \left(\frac{L}{\eta(G)}\right)^{D_F - 1}. \tag{16}$$

This model assumes that the flame is fractal between the viscous scale and the integral scale, L, as we justified in Section 5.1. The flame length has two contributions. The first term, L_{RT} is the large-scale stretching caused by the RT instability. Turbulent wrinkling, the second term, is superimposed on the stretched flame. All of the components of the second term are known, so the scaling of the first term can be determined from the second term and the scaling of the flame speed. We determined in the previous section that $D_F \to 1.5$ for large values of G. We also showed in Section 3 that Re $= L(1 + 0.205(G - G_1)L)^{0.558}$. Using the relation for the viscous scale in 2D turbulence, $\eta = L * \mathrm{Re}^{-1/2}$ with the previous two equations gives $L_f \propto L_{\mathrm{RT}}(G) * G^{0.14}$ for large values of G. We already know that $s \propto \sqrt{GL}$, so it follows that large-scale RT stretching scales as $G^{0.36}$ and the turbulent wrinkling scales as $G^{0.14}$. Therefore, for large values of G, large-scale RT stretching will contribute more to the flame speed than turbulent wrinkling. The dominant behavior of large scales again suggests that the RT subgrid model is an appropriate description for the flames we are studying.

What about 3D flames? In that case, the viscous scale is given by $\eta = L\mathrm{Re}^{-3/4}$ and $D_F \to 2.36$ for large values of G (see Section 5.1). Since we have not yet carried out simulations in 3D, we do not know the scaling for the Reynolds number in this regime. However, we can determine what the scaling would have to be in order for turbulent wrinkling to win out over large-scale RT stretching: Re $\propto G^{0.93}$. Based on our numerical results so far, this scaling shows what is probably an unrealistically large dependence on G (given that the 2D Reynolds number dependence only scales as $G^{0.558}$), which

would represent a hugely efficient generation of turbulence by the flame. Therefore, it is likely that in 3D RT stretching still dominates over turbulent wrinkling, a prediction that will need to be verified by future calculations.

An ordinary flame is subject to effects other than just RT stretching and turbulent wrinkling, specifically, flame stretch and curvature effects. These effects can destroy the usual proportionality between the flame surface area and the turbulent flame speed because the local flame speed is modified from its laminar value. For example, if the Lewis number is not equal to one, then the flame will be subject to stretch and strain effects due to the difference in thermal and material diffusivities (Dursi et al. 2003; Law 2006). The Lewis number of our flames is equal to one, so these effects are nonexistent. A flame can also be modified by pure curvature effects (Law 2006; Markstein 1964): in areas where the curvature of the flame is positive with respect to the fuel the local flame speed is smaller than the laminar flame speed and in areas where the curvature is negative the local flame speed is larger than the laminar flame speed (Markstein 1964). The total effect of these local changes to the flame speed can be taken into account by changing the laminar flame speed to a new value. However, this change will not affect the flame speed of the RT-driven flame (for large values of G) because the flame speed does not depend on the laminar flame speed (Khokhlov 1995); see Equation (4). This means that the scalings given above for the RT stretching and turbulent wrinkling are also not affected by curvature effects. The effect of Le $\neq 1$ can also be described as a change in the laminar flame velocity. So even in that case, the turbulent flame speed can still be divided into RT stretching and turbulent wrinkling alone, as long as no large-scale Le $\neq 1$ instabilities are present.

Given this argument, it is interesting to note that both Zingale et al. (2005a) and Bell et al. (2004) found that the surface area of their carbon–oxygen flames predicted a much higher flame speed than they actually found. This difference from our results could be due to the difference between their more realistic flames and our model flames, Lewis number effects beyond the local modification of the flame speed, or the difference between the transient regime (which they studied) and the saturated regime (studied here). We return to this point in Section 6 below.

In this subsection, we disentangled the effects of large-scale RT stretching and turbulent wrinkling on the flame front by finding their respective contributions to a fractal model of the flame speed. We found that large-scale RT stretching is the dominant contribution to the flame speed, and that it outweighs the contribution from turbulent wrinkling when G is large. We discussed local effects (flame stretch and curvature) that could invalidate a fractal flame model for the flame speed, and argued that these effects do not apply here. These results support the RT subgrid model because they show that the flame speed is controlled by the largest scales in the problem, as is expected in the formulation of the RT subgrid model.

6. CONCLUSIONS

In this paper, we contributed results from a fully resolved 2D parameter study of RT unstable flames in which we varied the non-dimensional gravity, G. This study extends the model flame results of Vladimirova & Rosner (2003, 2005) to much larger values of GL, for which the flame is significantly disrupted by turbulence. The main purpose of the study was to understand the interaction between the RT instability, the flame surface, and the turbulence behind the flame surface, and to use this

understanding to distinguish between the two major types of subgrid models: RT- and turbulence-based. We gave scalings for the turbulent flame speed, the Reynolds number, the viscous scale, and the height of the flame, and used these scalings to calculate the Karlovitz number, showing that, although we expect a transition from corrugated flamelets to thin reaction zones, we did not observe one. Finally, we calculated the fractal dimension of the flame, and showed that it approaches an asymptotic value of about $D_F = 1.5$; we used this result to develop a fractal-dimension model of the flame speed. Using this model, we demonstrated that the relative contributions of large-scale stretching to the flame speed are larger than the contributions of small- to mid-scale wrinkling.

Our conclusions from these calculations support the RT-based subgrid model. First, the turbulent flame speed scales with the RT flame speed, $s \propto \sqrt{GL}$. This alone is enough to confirm the RT subgrid model because the purpose of the model is the produce the correct flame speed. Second, the flame is fractal and is therefore self-similar, which confirms one of the two major requirements for the RT subgrid model. Finally, we observed that a larger percentage of the flame speed at large GL is due to large-scale stretching than to the small-scale wrinkling due to turbulence. This means that the flame is controlled by the large scales, as postulated by the RT subgrid model, instead of by the small scales, as postulated by turbulence-based subgrid models. In addition, we found evidence that traditional turbulent combustion models may not apply to the RT unstable flame system. In summary, we confirmed that the RT subgrid model produces the correct flame speed in 2D, and that its physical basis on the self-similarity and large-scale control of the flame is sound.

In addition, the result that the flame speed scales as the RT flame speed means that the flame will never achieve speeds near the sound speed in the white dwarf via this mechanism (Hillebrandt & Niemeyer 2000; Vladimirova & Rosner 2003). The fact that RT stretching contributes more to the flame speed than turbulent wrinkling suggests that there is no runaway wrinkling process that can occur for high GL that accelerates the flame past the RT flame speed. This means that the flame will be unable to transition to a detonation simply by increasing its surface area to reach the sound speed. Other mechanisms, such as the Zel'dovich gradient mechanism, are needed to actually cause a detonation.

By design, these simulations do not realistically match the conditions in the white dwarf. Most importantly, the simulations are in 2D. We know that 3D turbulence is very different from 2D turbulence. The key issue is the direction of the energy cascade, which in 3D takes energy from large scales to small scales. Exactly how this difference in energy cascade affects our results, in particular our discussion of the fractal nature of the flame, will only be answered by carrying out 3D simulations.

The second unrealistic characteristic of these simulations is that they are confined by the simulation box, while unconfined RT flames in an expanding star may behave differently. However, confined, saturated simulations can still be useful, because they indicate the statistically steady state the flame is working toward, even if it never reaches it. In addition, the self-regulating mechanism, which leads to a statistically steady flame speed in the saturated case studied here does not necessarily depend on saturation to operate (Zhang et al. 2007). This means that the results given in this paper may apply to the transient flame when the turbulence behind the flame is able to respond the RT instability sufficiently quickly.

Finally, these simulations were of a model flame while the actual flame is a carbon–oxygen nuclear flame. However, model flames are useful in two different ways. First, having a model flame allowed us to isolate the effect of gravity without worrying about Lewis number effects. Second, comparisons with carbon–oxygen nuclear flames show that there are intriguing differences between the two that could be due to Le effects or other characteristics of the nuclear flame. Specifically, we found that the fractal dimension in our case seems to asymptote to $D_F = 1.5$ while Bell et al. (2004) inferred indirectly that their flames were best described by $D_F = 1.7$. Also, in our simulations, the flames were well described by fractals, while Bell and Zingale found that the flame surface area overestimated the actual flame speed. Thus, comparisons with model flames could provide clues to the cause of certain characteristics of more realistic flames. In particular, the realistic Le $\neq$ 1 flames may be affected by thermo-diffusive instabilities that compete with the RT instability.

In the future, large-scale 3D simulations are needed to test whether the RT-based subgrid model for the flame speed does hold in 3D. Some results already indicate this is the case (Zhang et al. 2007). We plan to use this 2D study as a basis for a 3D study along these lines. If the RT flame speed does hold in 3D, then the stretching versus wrinkling argument in Section 5.2 will be validated. As we argued earlier, because the flame front behaves more and more like a passive scalar for high values of G, we expect the fractal dimension of the flame front to be inevitably bounded from above. This implies that, unless the production of turbulence by the flame in 3D is extremely efficient, RT stretching controls the flow and the RT-based subgrid model is the most appropriate subgrid model.

REFERENCES

Arnett, W. D. 1969, Ap&SS, 5, 180
Aspden, A. J., Bell, J. B., Day, M. S., Woosley, S. E., & Zingale, M. 2008, ApJ, 689, 1173
Aspden, A. J., Bell, J. B., Dong, S., & Woosley, S. E. 2011a, ApJ, 738, 94
Aspden, A. J., Bell, J. B., & Woosley, S. E. 2010, ApJ, 710, 1654
Aspden, A. J., Bell, J. B., & Woosley, S. E. 2011b, ApJ, 730, 144
Aspden, A. J., Day, M. S., & Bell, J. B. 2011c, JFM, 680, 287
Bell, J. B., Day, M. S., Rendleman, C. A., Woosley, S. E., & Zingale, M. 2004, ApJ, 608, 883
Blinnikov, S. I., & Sasorov, P. V. 1996, PhRvE, 53, 4827
Bravo, E., & Garcia-Senz, D. 1995, ApJL, 450, L17
Bychkov, V., & Liberman, M. 2000, PhR, 325, 115
Chertkov, M., Lebedev, V., & Vladimirova, N. 2009, JFM, 633, 1

Ciaraldi-Schoolmann, F., Schmidt, W., Niemeyer, J. C., Röpke, F. K., & Hillebrandt, W. 2009, ApJ, 696, 1491
Collins, L. R. 1995, Ind. Eng. Chem. Res., 2588
Constantin, P., Kiselev, A., & Ryzhik, L. 2003, CPAM, 56, 1781
Constantin, P., Procaccia, I., & Sreenivasan, K. R. 1991, PhRvL, 67, 1739
Damkohler, G. 1940, (trans. 1947), Z. Elektrochem (trans. in Technical Memorandums, United States, National Advisory Committee for Aeronautics.), 46 (trans. 1112), 601
Davidson, P. A. 2004, Turbulence: An Introduction for Scientists and Engineers (Oxford: Oxford Univ. Press)
Dursi, L. J., Zingale, M., Calder, A. C., et al. 2003, ApJ, 595, 955
Filippenko, A. 1997, ARA&A, 35, 309
Fischer, P. F., Lottes, J. W., & Kerkemeier, S. G. 2008, Nek5000 Web page, http://nek5000.mcs.anl.gov
Foroutan-pour, K., Dutilleul, P., & Smith, D. L. 1999, ApMaC, 105, 195
Gamezo, V. N., Khokhlov, A. M., & Oran, E. S. 2004, PhRvL, 92, 211102
Gamezo, V. N., Khokhlov, A. M., & Oran, E. S. 2005, ApJ, 623, 337
Gamezo, V. N., Khokhlov, A. M., Oran, E. S., Chtchelkanova, A. Y., & Rosenberg, R. O. 2003, Sci, 299, 77
Gamezo, V. N., Wheeler, J. C., Khokhlov, A. M., & Oran, E. S. 1999, ApJ, 512, 827
Gouldin, F. 1987, CoFl, 68, 249
Gulder, O. 1990, in Symposium (International) on Combustion, 23, 835
Gulder, O. 1999, in Proc. Mediterranean Combustion Symposium-99 (MCS-99), Antalya, Turkey, 1999 June 20–25 (Naples, Italy: Tipolitografia Enzo Albano), 130
Hamlington, P. E., Poludnenko, A. Y., & Oran, E. S. 2011, PhFl, 23, 125111
Hamlington, P. E., Poludnenko, A. Y., & Oran, E. S. 2012, PhFl, 24, 075111
Hillebrandt, W., & Niemeyer, J. C. 2000, ARA&A, 38, 191
Jordan, I. G. C., Fisher, R. T., Townsley, D. M., et al. 2008, ApJ, 681, 1448
Kerstein, A. 1988, CST, 60, 441
Khokhlov, A., Mueller, E., & Hoeflich, P. 1993, A&A, 270, 223
Khokhlov, A. M. 1995, ApJ, 449, 695
Khokhlov, A. M., Oran, E. S., & Thomas, G. 1999, CoFl, 117, 323
Khokhlov, A. M., Oran, E. S., & Wheeler, J. C. 1996, CoFl, 105, 28
Khokhlov, A. M., Oran, E. S., & Wheeler, J. C. 1997, CoFl, 108, 503
Krueger, B. K., Jackson, A. P., Calder, A. C., et al. 2012, ApJ, 757, 175
Law, C. K. 2006, Combustion Physics (Cambridge: Cambridge Univ. Press)
Layzer, D. 1955, ApJ, 122, 1
Mandelbrot, B. 1967, Sci, 156, 636
Mandelbrot, B. B. 1982, The Fractal Geometry of Nature (San Francisco, CA: Freeman)
Mantzaras, J., Felton, P., & Bracco, F. 1989, CoFl, 77, 295
Markstein, G. (ed.) 1964, Non-Steady Flame Propagation (New York: Macmillan)

Niemeyer, J., & Hillebrandt, W. 1995, ApJ, 452, 769
Niemeyer, J. C., & Kerstein, A. R. 1997, NewA, 2, 239
Niemeyer, J. C., & Woosley, S. E. 1997, ApJ, 475, 740
Nonaka, A., Aspden, A. J., Zingale, M., et al. 2012, ApJ, 745, 73
Oran, E. S. 2005, in Proc. Combustion Institute, 30, 1823
Oran, E. S., & Gamezo, V. N. 2007, CoFl, 148, 4
Peters, N. 2000, Turbulent Combustion (Cambridge: Cambridge Univ. Press)
Poludnenko, A. Y., Gardiner, T. A., & Oran, E. S. 2011, PhRvL, 107, 054501
Poludnenko, A. Y., & Oran, E. S. 2010, CoFl, 157, 995
Pope, S. B. 2000, Turbulent Flows (Cambridge: Cambridge Univ. Press)
Prasad, R. R., & Sreenivasan, K. R. 1989, ExFl, 7, 259
Reinecke, M., Hillebrandt, W., Niemeyer, J. C., Klein, R., & Gröbl, A. 1999, A&A, 347, 724
Röpke, F. K. 2007, ApJ, 668, 1103
Röpke, F. K., & Hillebrandt, W. 2005, A&A, 431, 635
Röpke, F. K., & Niemeyer, J. C. 2007, A&A, 464, 683
Schmidt, W., Niemeyer, J. C., & Hillebrandt, W. 2006a, A&A, 450, 265
Schmidt, W., Niemeyer, J. C., Hillebrandt, W., & Röpke, F. K. 2006b, A&A, 450, 283
Seitenzahl, I. R., Ciaraldi-Schoolmann, F., Röpke, F. K., et al. 2013, MNRAS, 429, 1156
Sharp, D. 1984, PhyD, 12, 3
Spiegel, E., & Veronis, G. 1960, ApJ, 131, 442
Sreenivasan, K. 2004, Flow Turbul. Combust., 72, 115
Sreenivasan, K. R. 1991, AnRFM, 23, 539
Sreenivasan, K. R., & Meneveau, C. 1986, JFM, 173, 357
Sreenivasan, K. R., Ramshankar, R., & Meneveau, C. 1989, RSPSA, 421, 79
Townsley, D. M., Calder, A. C., Asida, S. M., et al. 2007, ApJ, 668, 1118
Vladimirova, N. 2007, CTM, 11, 377
Vladimirova, N., Constantin, P., Kiselev, A., Ruchayskiy, O., & Ryzhik, L. 2003, CTM, 7, 487
Vladimirova, N., & Rosner, R. 2003, PhRvE, 67, 066305
Vladimirova, N., & Rosner, R. 2005, PhRvE, 71, 067303
Woosley, S. E. 1990, in Supernovae, ed. A. G. Petschek (Astronomy and Astrophysics Library; New York: Springer)
Woosley, S. E., Kerstein, A. R., & Aspden, A. J. 2011, ApJ, 734, 37
Zel'dovich, Y. B., Librovich, V. B., Makhviladze, G. M., & Sivashinskil, G. I. 1970, JAMTP, 11, 264
Zhang, J., Bronson Messer, O. E., Khokhlov, A. M., & Plewa, T. 2007, ApJ, 656, 347
Zingale, M., & Dursi, L. J. 2007, ApJ, 656, 333
Zingale, M., Woosley, S. E., Bell, J. B., Day, M. S., & Rendleman, C. A. 2005a, JPhCS, 16, 405
Zingale, M., Woosley, S. E., Rendleman, C. A., Day, M. S., & Bell, J. B. 2005b, ApJ, 632, 1021